

# Efficient liposome fusion to phase-separated giant vesicles

Rafaela R. M. Cavalcanti,<sup>1,2</sup> Rafael B. Lira,<sup>2</sup> Eleanor J. Ewins,<sup>2</sup> Rumiana Dimova,<sup>2,\*</sup> and Karin A. Riske<sup>1,\*</sup>

<sup>1</sup>Department of Biophysics, Universidade Federal de São Paulo, São Paulo, Brazil and <sup>2</sup>Max Planck Institute of Colloids and Interfaces, Science Park Golm, Potsdam, Germany

**ABSTRACT** Lateral phase heterogeneity in biomembranes can govern cellular functions and may serve as a platform for enrichment or depletion of membrane-anchored molecules. In this work, we address the question of how the process of membrane fusion is affected by the membrane phase state (fluid or gel) and by phase coexistence, as well as the effects of fusion-mediated incorporation of exogenous lipids on phase separation. Our system is based on the fusion of cationic fluid large unilamellar vesicles (LUVs) composed of dioleoyl trimethylammonium propane (DOTAP) and dioleoyl phosphoethanolamine (DOPE) with neutral and anionic giant unilamellar vesicles (GUVs) composed of phosphatidylcholine and phosphatidylglycerol. By changing the lipid composition of the GUVs, we modulated the phase state and charge of the different phases (charged or neutral, fluid or gel) and identified systems in which we can target fusion to specific domains on phase-separated membranes. Fusion efficiency was quantified using fluorescence microscopy-based lipid and content mixing assays, and flow chamber devices were used to assess the real-time sequence of events of the fusion process. To investigate the bilayer thermal behavior, differential scanning calorimetry (DSC) experiments were performed on LUVs. The results show that fusion is extensive in single-component GUVs only for fluid and negatively charged acceptor membranes. On the other hand, in phase-separated GUVs, high fusion efficiency was observed even when the gel phase was anionic and phase separation somewhat increased the fusion efficiency. Extensive fusion led to dissolution of the gel domains as a result of extensive incorporation of lipids in the fluid state from the fusogenic liposomes. Altogether, these findings have the potential to unravel the important role of membrane phase state, phase separation, charge, and the effects of extensive fusion on membrane organization and may give insights in the regulation of the interactions between cells and liposomes that are used in drug delivery systems.

**SIGNIFICANCE** Membrane fusion is a vital process for cell communication, trafficking, and signaling, in which two membranes come into close contact and eventually merge, connecting the two initially separated aqueous compartments. Beyond its physiological importance, fusion has also a great potential as a drug delivery route, avoiding the slow and inefficient endocytic-based pathways. In cells, fusion relies on a complex protein machinery. Here we explored the protein-free fusion of cationic liposomes to giant unilamellar vesicles exhibiting gel-fluid phase separation in which one phase is negatively charged. Our predominant focus was to elucidate the role of membrane heterogeneity in the fusion process and target fusion to a specific domain.

## INTRODUCTION

Membrane fusion is a result of the merging of two membranes and leads to mixing of the otherwise separated aqueous compartments. It is essential for maintaining the viability of cells and organisms, and has long been known to play a crucial role in a wide variety of processes,

including egg fertilization, development of muscles, intracellular trafficking, and release of hormones and neurotransmitters (1–4). Membrane fusion is also fundamental to the entrance of envelope viruses in cells, e.g., HIV-1, Ebola virus, influenza, and severe acute respiratory syndrome coronavirus-2 (SARS-CoV-2) (5,6) and in developing vaccines against them. Although involved in seemingly different processes, fusion follows common and well-defined pathways. It proceeds through general intermediate steps such as docking (adhesion of opposing membranes); mixing of lipids from the outer leaflets of the opposing membranes, while the inner membranes are still separated

Submitted June 28, 2022, and accepted for publication December 2, 2022.

\*Correspondence: rumiana.dimova@mpikg.mpg.de or kariske@unifesp.br

Rafael B. Lira and Eleanor J. Ewins's present address is Zernike Instituut, Rijksuniversiteit Groningen, Groningen, the Netherlands.

Editor: Erdinc Sezgin.

<https://doi.org/10.1016/j.bpj.2022.12.008>

© 2022 Biophysical Society.



(hemifusion); and the formation and expansion of the fusion neck (full fusion) (7,8). Upon full fusion, the fused vesicles/cells have fully mixed their lipids and membrane proteins as well as the originally separated aqueous contents (9). In addition to its involvement in normal cell physiological processes, membrane fusion can also be used as a route for drug delivery. For decades, lipid vesicles (also known as liposomes) have been used as one of the most popular drug-carrier vehicles for intracellular delivery of cargos (i.e., small molecules, proteins, nanoparticles) (10,11). However, they usually enter the cells via endocytosis, a slow and often inefficient pathway that is dependent on the ability of cells to internalize particles and that could potentially damage the cargo in the low pH of endocytic organelles (12–14). As a possible way to circumvent internalization-dependent pathways, direct fusion of liposomes with cells offers an alternative for fast and efficient intracellular delivery as they can potentially release the encapsulated material directly into the cytosol without the need of endocytosis, and, thus, fusogenic liposomes could fulfill this role. One such type of fusogenic liposome is based on cationic large unilamellar vesicles (LUVs) composed of positively charged dioleoyl trimethylammonium propane (DOTAP) and the helper, zwitterionic, non-bilayer-forming lipid dioleoyl phosphatidylethanolamine (DOPE), along with a fraction of fluorescent lipids. These LUVs fuse with a large variety of cells and tissues and have been used for the delivery of lipids, proteins, and nanoparticles into cells (15–18). They have the advantage of being compositionally simple, and yet able to fuse efficiently without the need of complex functionalization moieties.

Since membrane fusion in living cells is a complex and dynamic process and involves many regulatory proteins, simplified assays using biomimetic systems have been established to understand its molecular details (19–21). Such systems allow for precise control of the membrane and environmental components while avoiding the influence of peripheral processes that are only marginally associated with fusion. In this regard, the use of giant unilamellar vesicles (GUVs) in studies of membrane fusion grant a number of advantages that are difficult (or even impossible) to obtain with other model membranes (21). Single GUVs can be tracked and manipulated with microscopy-based approaches, and this allows quantification of important fusion parameters, such as fusion efficiency, kinetics, and possible disruptive effects on single vesicles with controlled membrane composition (21,22). Recently, using cationic DOTAP:DOPE liposomes, we quantified the fusion efficiency and studied the role of charges on fusion with GUVs by varying the fraction of the charged lipid palmitoyl oleoyl phosphatidylglycerol (POPG) in GUVs containing the zwitterionic lipid palmitoyl oleoyl phosphatidylcholine (POPC) (22). We showed that LUVs dock and predominantly undergo hemifusion with GUVs composed of pure POPC or low fractions of POPG, whereas, above 20 mol% POPG, we observe extensive fusion

associated with a substantial increase in the surface area of GUVs (22). Furthermore, charge-mediated fusion was found to be a strongly exothermic process occurring concomitantly with charge neutralization (23).

In addition to membrane charges, the membrane phase state could potentially influence membrane fusion, promoting or hindering it (24–26). The lipids that constitute the cell membrane have different forms of organization and therefore may give rise to heterogeneous membranes (27–29). This heterogeneity can be related to how lipids are structurally and dynamically organized. Depending on the composition and the temperature, pure lipid bilayers can be found in the gel (solid-ordered) or fluid (liquid-disordered) phases. Addition of cholesterol can lead to the appearance of the liquid-ordered phase (30,31). For single-component membranes, the transition between the gel and fluid phases occurs at a main transition temperature ( $T_m$ ) that is particular for each lipid and is highly dependent on the chain length, degree of unsaturation, and on the lipid polar head-group (32). Long-chain saturated lipid bilayers, such as dipalmitoyl phosphatidylcholine (DPPC, zwitterionic) and dipalmitoyl phosphatidyl glycerol (DPPG, anionic), have a high  $T_m$  at 41°C (33); however, the presence of unsaturation dramatically reduces the  $T_m$  (e.g., for POPC and POPG lipids,  $T_m$  is around –2°C; (34)). Most natural lipids have one saturated and one unsaturated chain and are therefore found in the fluid phase at physiological temperature (35,36). Several sphingolipids, such as sphingomyelin, have long and saturated chains and are therefore in the gel phase at room and physiological temperatures. In fact, phase separation in both liposomes (using synthetic lipids with different  $T_m$ ) and cell membranes (presence of lipid rafts) systems have been shown to favor membrane fusion (37,38). Strikingly, the presence of defects associated with phase separation was shown to be more important for membrane fusion than the specific membrane phase, favoring binding and fusion of virus-like liposomes to phase-separated GUVs (39,40). However, the molecular details that influence membrane fusion in phase-separated systems, the preferential binding to a specific region of the membrane, and most importantly the mechanical and thermodynamic effects of fusion on membrane phase state are still unknown.

Our main motivation is to explore the interdependence of fusion efficiency and of membrane phase state in homogeneous membranes and, more importantly, in phase-separated membranes. Here we study membrane fusion between fusogenic DOTAP:DOPE LUVs (~100 nm) with single-component GUVs (POPC, POPG, DPPC, and DPPG) in different phases and charge state and with GUVs exhibiting gel-fluid phase coexistence in which one of the phases is negatively charged (POPC:DPPG and POPG:DPPC). We used confocal fluorescence microscopy to assess LUV docking and fusion to GUVs. To investigate the thermal behavior of the mixtures, differential scanning calorimetry (DSC) experiments were performed.

## MATERIALS AND METHODS

### Materials

The lipids 1-palmitoyl-2-oleoyl-sn-glycero-3-phosphocholine (POPC), 1-palmitoyl-2-oleoyl-sn-glycero-3-phospho-1'-rac-glycerol (POPG), 1,2-dipalmitoyl-sn-glycero-3-phosphocholine (DPPC), 1,2-dipalmitoyl-sn-glycero-3-phospho-(1'-rac-glycerol) (DPPG), 1,2-dioleoyl-3-trimethylammonium propane (DOTAP), 1,2-dioleoyl-sn-glycero-3-phosphoethanolamine (DOPE), and the fluorescent dyes 1,2-dipalmitoyl-sn-glycero-3-phosphoethanolamine-N-(lissamine rhodamine B sulfonyl) (ammonium salt) (DPPE-Rh) and 1,2-dipalmitoyl-sn-glycero-3-phosphoethanolamine-N-(7-nitro-2-1,3-benzoxadiazol-4-yl) ammonium salt (DPPE-NBD) were purchased from Avanti Polar Lipids (Alabaster, AL). The water-soluble fluorescence dye ATTO 647 (ATTO) was purchased from Atto-Tec (Siegen, Germany) and diluted in DMSO. Sucrose and glucose were purchased from Sigma Aldrich (St. Louis, MO).

### Preparation of lipid vesicles

Cationic LUVs composed of DOTAP:DOPE (1:1) were used as fusogenic liposomes and acceptor membranes consisted of GUVs composed of pure POPC, POPG, DPPC, and DPPG or of the mixtures POPC:DPPG (1:1) and POPG:DPPC (1:1). The lipid dyes and its concentration varied within each experiment and therefore are described together with the experiments. For the formation of LUVs, a film from a lipid solution in chloroform was deposited inside a glass vial by evaporation of the organic solvent with N<sub>2</sub>. This tube was then placed in vacuum for 2 h to evaporate remaining traces of the solvent. Afterward, an aqueous solution of 0.2 M sucrose or glucose was added, and the test tube was vortexed for 1 min to form multilamellar vesicles (MLVs). To obtain LUVs, the MLV suspension were extruded at least 13 times through a 100-nm polycarbonate membrane in a mini-extruder (Avanti Polar Lipids, Alabaster, AL) (41). When preparing LUVs for content mixing assays, 20 μM ATTO 647 was added to the aqueous solution before hydrating the dried lipid film. The LUVs stock suspension was diluted at least 10 times before addition to the GUVs to ensure that the ATTO 647 concentration inside the LUVs was significantly higher than in the external medium.

GUVs were prepared by the electroformation method. Briefly, 8–10 μL of a 3 mM lipid solution in chloroform were spread on the surfaces of two conductive glass plates coated with a thin layer of indium tin oxide (ITO) or fluor tin oxide (FTO). After evaporation of the organic solvent with N<sub>2</sub>, the two plates were sealed with a 1-mm-thick Teflon spacer between them forming a ≈2-mL chamber. Thereafter, approximately 1 mL of 0.2 M sucrose solution was added to the chamber and the plates were connected to a function generator. An alternating voltage source of either 1.8 V or 2.6 V amplitude (for homogenous and heterogeneous GUVs, respectively) and 10 Hz frequency was applied for 1 h. The growth process was performed in the dark and inside an oven at 50°C whenever DPPC or DPPG was present. After the incubation time, the door of the oven was kept open for 20 min and the GUV suspension was then transferred to a test tube that was then kept at room temperature for at least 10 min to allow the GUVs to slowly cool down. Then, the GUVs were diluted approximately 10-fold in 0.2 M glucose solution to increase the optical contrast when observed under phase contrast microscopy.

### Observation of GUVs and LUVs using optical microscopy

Confocal microscopy experiments were performed on a Leica TCS SP5 or SP8 (Wetzlar, Germany) equipped with 40× air (numerical aperture [NA] 0.6) and 63× water (NA 1.2) immersion objectives. Vesicles (LUVs and GUVs) were fluorescently labeled with 0.5 mol % or 1 mol % DPPE-

NBD DPPE-Rh membrane dyes, and they were excited with an argon laser at 488 nm (emission 495–550 nm) and a diode-pumped solid-state laser at 561 nm (emission 570–660 nm), respectively. The exact concentrations of the membrane dyes are described in each figure caption. For Förster resonance energy transfer (FRET), a 488-nm excitation and emission at 495–550/570–660 nm was used. For content mixing, a HeNe 633 laser was used to detect the hydro soluble dye (ATTO 647) at 633/660–680nm (excitation/emission). Phase contrast experiments were performed on a Zeiss Axiovert 200 (Jena, Germany) inverted microscope equipped with 40× (NA 0.6) and 63× (NA 0.75) air objectives and coupled to a PCO.edge 4.2 digital camera (Kelheim, Germany).

### FRET assay

A method based on the FRET intensity was used to quantify fusion efficiency between fusogenic LUVs and single-component GUVs (22). The FRET pair used was DPPE-NBD (donor) and DPPE-Rh (acceptor). GUVs were labeled with 0.5 mol % DPPE-NBD and fusogenic LUVs contained 1 mol % DPPE-Rh. Fusogenic LUVs and homogenous GUVs composed of POPC, POPG, DPPC, and DPPG were incubated for 15 min. Then, the FRET efficiency ( $E_{\text{FRET}}$ ) was measured from the membrane fluorescence intensities of the donor ( $I_D$ ) and acceptor ( $I_A$ ) channels when only DPPE-NBD was excited:

$$E_{\text{FRET}} = \frac{I_A}{(I_D + I_A)}$$

Depending on how efficient membrane fusion was, the  $E_{\text{FRET}}$  values varied from 0 (no membrane fusion) to 1 (high membrane fusion efficiency).

Quantification of the fluorescence intensity in the DPPE-Rh channel was performed using the LAS X software. Contour lines were drawn along the outer and inner sides of the GUV membrane and the fluorescence intensity value within the two contour lines was used to quantify the total amount of transferred lipid (Fig. 1 C).

### Flow chamber for single-vesicle analysis

A sticky-Slide I 0.4 Luer (Ibidi) flow chamber was used to observe changes in the same GUV upon controlled injection of LUVs in the solution. The chamber coverslip was coated with 2 mg/mL casein to avoid the excessive binding of LUVs onto the glass. The flow chamber coupled to a neMESYS syringe pump (Cetoni, Germany) was mounted on a confocal microscope (SP8, Leica). The chamber's channel and reservoirs were completely filled with 232.5 μL of 0.2 M glucose. After removing 70 μL of solution from the reservoir of the chamber, 70 μL of GUVs labeled with 0.5 mol % DPPE-Rh were added in the reservoir and introduced in the channel with a flow of 20 μL/min for 2 min. After a few minutes, the GUVs had settled to the glass surface as a result of the sucrose/glucose asymmetry imposed to the GUV. Then, 40 μL of a dispersion of LUVs (210 μM lipid concentration labeled with 1 mol % DPPE-NBD) encapsulating 20 μM ATTO 647 (≈2 μM ATTO 647 on the outside) were added in the reservoir and introduced at a fixed flow of approximately 2 μL/min. The flow was stopped once the LUVs were close to the GUV of interest and the first hints of fusion were detected (e.g., green fluorescence on the GUV surface). Then z stack images of GUVs were taken at every 2–3 min to follow changes in a single GUV from when the LUVs had initially arrived at the surroundings of the GUV until the total dissolution of the domains.

### DSC

The thermal profiles of LUVs with different compositions were performed using the MicroCal PEAQ-DSC. The reference cell was filled with 250 μL of 0.2 M glucose and the sample cell was filled with 250 μL of LUVs

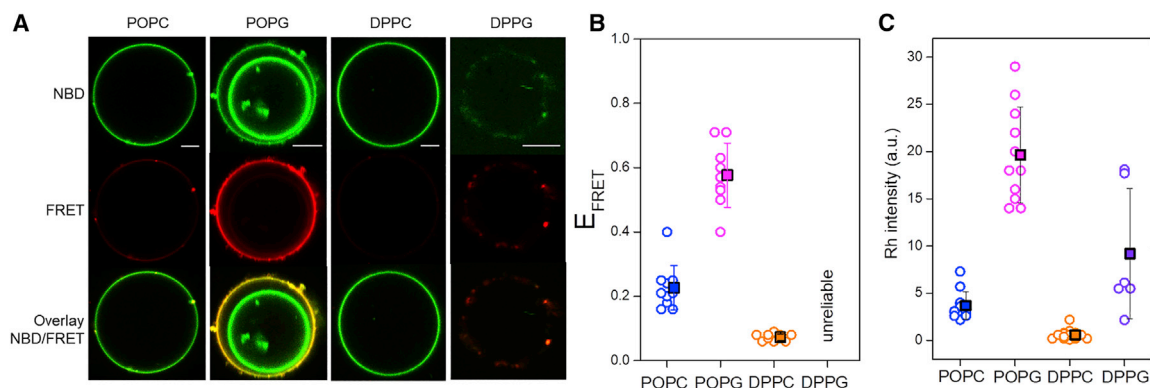


**FIGURE 1** Lipid mixing due to fusion is strongly affected by the phase state and charge of single-component membranes. FRET efficiency ( $E_{\text{FRET}}$ ) for single-component GUVs composed of POPC, POPG, DPPC, and DPPG with 0.5 mol % DPPE-NBD after 15-min incubation with fusogenic LUVs (20 μM DOTAP:DOPE with 1 mol % DPPE-Rh). (A) Representative confocal microscopy images of GUVs obtained after incubation with fusogenic LUVs. Top row, DPPE-NBD channel; middle row, FRET channel (DPPE-Rh fluorescence upon DPPE-NBD excitation); bottom row, overlay of both channels. Scale bars, 5 μm. (B)  $E_{\text{FRET}}$  values measured on GUVs. Each open circle represents a measurement on a single GUV and solid squares are mean values with SD.  $E_{\text{FRET}}$  values could not be measured in the DPPG system. (C) Fluorescence intensity of the DPPE-Rh channel (DPPE-Rh fluorescence upon DPPE-Rh excitation; in arbitrary units) measured over the whole contour of the GUVs, which reflects the amount of lipids transferred upon fusion. Each open circle represents a measurement on a single GUV and solid squares are mean values with standard deviation (SD). To see this figure in color, go online.

composed of 5 mM total lipid concentration of: POPG:DPPC (1:1), POPC:DPPG (1:1), DOTAP:DOPE (1:1), POPG:DPPC:DOTAP:DOPE (1:1:1:1), and POPC:DPPG:DOTAP:DOPE (1:1:1:1). DSC measurements of LUVs composed of 5 mM POPC:DPPG (1:1) and 5 mM POPG:DPPC (1:1) were also taken after 20 min of incubation with 5 mM DOTAP:DOPE (1:1) LUVs in a 1:1 volume ratio. The temperature range was 2–60°C at a scan rate of 20°C/h (heating). Baseline subtraction was performed in Microcal Origin 7.0. The thermograms are shown as molar heat capacities considering only the concentration of DPPC or DPPC lipids in the mixture.

## RESULTS

Membrane fusion between fusogenic LUVs (~100 nm) composed of equimolar fractions of DOTAP (cationic) and DOPE (zwitterionic) with GUVs with different phase states (gel or fluid) and charge (zwitterionic or negative) was assessed using a variety of optical microscopy techniques and DSC. Fusion was investigated in single-component and in phase-separated GUVs of different charges after incubation with increasing concentrations of LUVs and quantitatively assessed with intensity-based FRET on single-component GUVs. For phase-separated GUVs, fusion efficiency was quantified by the transfer of fluorescent probes incorporated in the LUVs or encapsulated in their inner compartment and the dynamics of the fusion process was tracked using a flow chamber. Last, the thermal behavior of the lipid mixtures before and after fusion was analyzed using DSC.

### Fusion of LUVs with single-component GUVs

GUVs composed of pure lipids (POPC, POPG, DPPC, or DPPG), forming respectively neutral fluid, charged fluid, neutral gel, and charged gel membranes, were prepared and incubated with fusogenic LUVs (20 μM lipid concentra-

tion). Fusion efficiency was quantified by a lipid-mixing assay in a FRET configuration (22) as explained in the “materials and methods” section. The membrane dye DPPE-NBD was incorporated in the GUVs and served as a FRET donor, and the LUVs were prepared with the membrane probe DPPE-Rh as a FRET acceptor. However, GUVs of pure DPPG were difficult to grow. Representative confocal microscopy images of GUVs after incubation with LUVs are shown in Fig. 1 A. Significant FRET signal was observed only for POPG, whereas the very few obtained DPPG vesicles exhibited bright spots in which both donor and acceptor probes were found enriched. Fig. 1 B shows  $E_{\text{FRET}}$  values calculated for several GUVs. POPC GUVs incubated with the fusogenic LUVs show a small but detectable  $E_{\text{FRET}}$  ( $0.20 \pm 0.09$ ), indicative of low fusion efficiency, consistent with previous results (22). In sharp contrast, incubation of fusogenic LUVs with GUVs composed of POPG led to a large increase in  $E_{\text{FRET}}$  ( $0.58 \pm 0.09$ ), as expected for highly negative membranes (22). Although Lira et al. (22) labeled the fusogenic LUVs with 5 mol % DPPE-Rh, the FRET experiments performed here used only 1 mol % DPPE-Rh. This explains the lower  $E_{\text{FRET}}$  values observed here compared with Lira et al. (22). As seen in Fig. 1 A, fusion is restricted to the bilayer in contact with the LUVs, whereas the membranes of internal vesicles remain inaccessible. When the LUVs are incubated with neutral gel GUVs composed of DPPC,  $E_{\text{FRET}}$  ( $0.07 \pm 0.01$ ) is much lower than with fluid-neutral POPC, suggesting that practically no fusion occurred. For DPPG vesicles,  $E_{\text{FRET}}$  could not be reliably obtained, as the vesicles exhibited a lower amount of incorporated DPPE-NBD before incubation with the fusogenic LUVs (about four times less than the other compositions) and a very heterogeneous distribution of probes was observed

after incubation, as can be seen in the different example in Fig. S1, which shows images of DPPG GUVs with enhanced contrast. The bright spots observed on the membrane surface of DPPG were detected in all channels (green, red, and FRET), which makes their interpretation hard. The heterogeneous presence of DPPE-Rh on the membrane surface suggests docking of LUVs onto the negative gel membrane; however, it is not clear why DPPE-NBD is also found enhanced in these regions and whether effective fusion could have occurred. The presence of this punctate fluorescence could be a result of events at disclination defects in the gel membrane. To compare the amount of fluorescent lipids transferred from the LUVs through fusion to the surface of the GUVs, we quantified the fluorescence intensity in the DPPE-Rh channel integrated along the contour of all GUVs, since for DPPG a very heterogeneous distribution was obtained. The results are shown in Fig. 1 C. The trend observed for POPC, POPG, and DPPC is similar to that observed from the  $E_{\text{FRET}}$  values (Fig. 1 B). The values found for the few DPPG vesicles show a large scatter and a mean value between those found for POPC and POPG. However, there is no unambiguous sign of membrane fusion, and the relatively high intensity probably points to docking and/or membrane defects. These results show that both membrane

charge and phase state play important roles in the fusion of fluid membranes.

### Fusion of LUVs with phase-separated GUVs

Lipid-mixing experiments with homogenous GUVs showed that significant full fusion was only observed when the GUVs were negatively charged and in the fluid state. Before analyzing fusion with binary mixtures, we first characterized the phase separation in GUVs composed of POPC:DPPG (1:1) and POPG:DPPC (1:1) in the absence of the fusogenic LUVs. Representative images of these two systems are shown in Figs. S2 and 2 (first images, 0  $\mu\text{M}$ ), in which equatorial views and 3D projection (Fig. S2) or top view (Fig. 2) are shown. The fluorescence dye used, DPPE-Rh, preferentially partitions in the fluid phase (42) and thus phase separation in GUVs is seen by the presence of red (fluid phase) and dark (gel phase) regions. Interestingly, the domain shape of the two GUV compositions is different: POPC:DPPG exhibits flower- or star-like domains (Figs. 2 A and S2 A), similar to those previously observed in POPC:DPPC (43) and DOPC:DPPG (44), whereas POPG:DPPC displays a coexistence of fluid stripes and faceted domains (Figs. 2 B and S2 B) similar

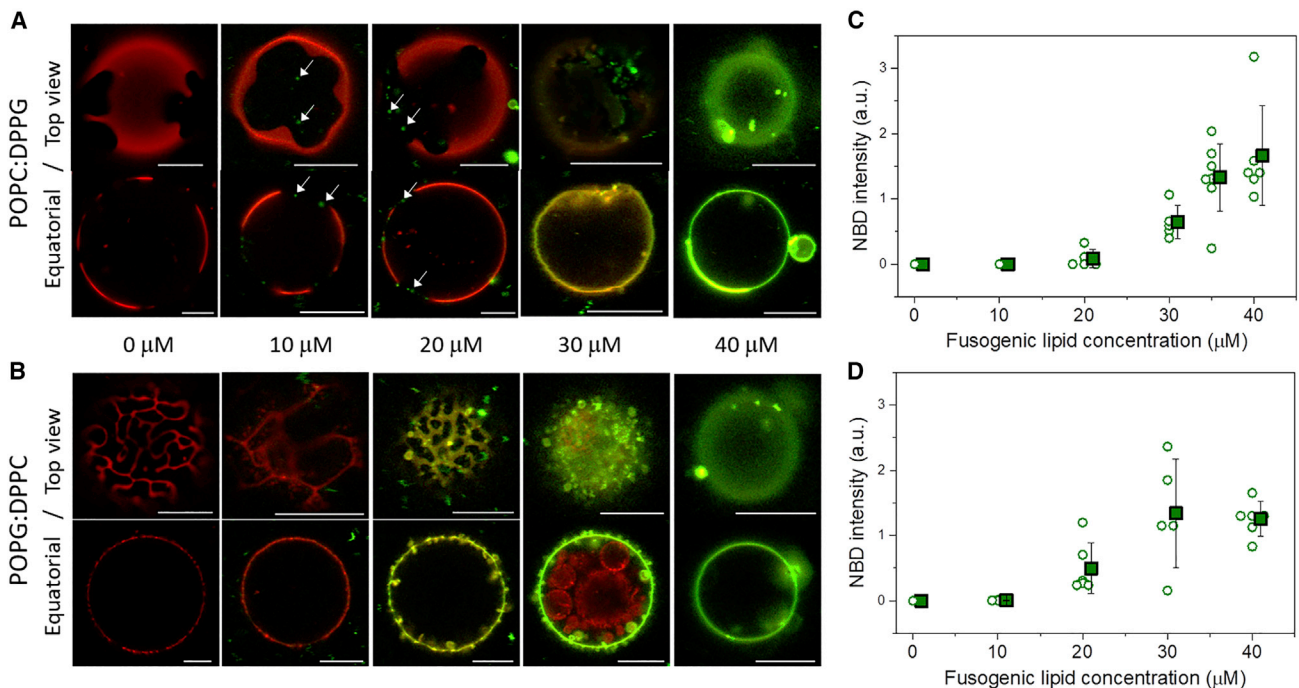


FIGURE 2 Increasing concentrations of fusogenic LUVs suppress the phase separation on GUVs with fluid and gel domains. Overlay of DPPE-NBD and DPPE-Rh channels obtained with confocal microscopy of phase-separated GUVs composed of (A) POPC:DPPG and (B) POPG:DPPC with 0.5 mol % DPPE-Rh after 10–15-min incubation with fusogenic LUVs (DOTAP:DOPE with 1 mol % DPPE-NBD) in increasing concentrations (0–40  $\mu\text{M}$  lipid). For each composition, both equatorial (bottom) and top view (top; image collected with an open pinhole) are shown. The white arrows displayed in (A) indicate docking of positively charged LUVs onto the negatively charged gel region of the GUV membrane. The images were processed (brightness, +40%, and contrast, +20%) to enhance the observation of the details. Scale bars, 5  $\mu\text{m}$ . The intensity of transferred DPPE-NBD to GUVs (arbitrary units) are shown in (C) for POPC:DPPG and (D) POPG:DPPC for increasing fusogenic lipid concentration. Each circle represents one GUV (5–7 GUVs were observed per fusogenic lipid concentration) and mean values and SD are shown as squares. The images for POPG:DPPC GUVs after incubation with 10 and 20  $\mu\text{M}$  fusogenic lipids were acquired with a threefold higher laser power, therefore the fluorescence intensity measured was divided by 3. To see this figure in color, go online.

to shapes characteristic for DLPC:DPPC GUVs (45). Such morphologies were detected for the vast majority of GUVs from several different preparations. For the POPC:DPPG membranes, the dark domains preserved their shapes over time (consistent with their gel phase state) but could diffuse along the GUV surface (consistent with fluid phase environment). The linear domains in the POPG:DPPC vesicles were rather static because the matrix phase was in the gel phase. It has been shown previously that larger mismatch between lipids and thus higher cost for boundaries could explain these different domain shapes (45,46). Additionally, DPPG was found to enhance and DOPG to suppress phase separation in ternary mixtures containing, respectively, DOPC and DPPC (44).

Next, we investigated the fusion of LUVs with phase-separated GUVs. GUVs were labeled with DPPE-Rh (red) and the LUVs with DPPE-NBD (green), and the fluorescence signal of each dye was observed separately in different channels. Precise measurements of  $E_{\text{FRET}}$  could not be performed due to the difficulties in resolving domain fractions in each GUV, and hence the data shown are based on the amount of DPPE-NBD green fluorescence transferred to the GUVs upon fusion with the LUVs. Two microscopy approaches were used. First, GUVs were incubated with increasing concentrations of LUVs and the outcome was observed under confocal microscopy. In the second approach, a flow chamber was used to follow changes in individual GUVs over time after addition of fusogenic LUVs. In the latter experiment, the LUVs were loaded with an aqueous soluble dye to assess content mixing.

#### *Pre-incubation of GUVs with fusogenic LUVs*

The two binary GUV compositions, POPC:DPPG (1:1) and POPG:DPPC (1:1), were incubated for 10–15 min with increasing concentrations of fusogenic LUVs (0–40  $\mu\text{M}$  lipid) to study the gradual effects of membrane fusion. Representative images of both compositions of GUVs for all LUV concentrations studied are shown as equatorial and top view projections in Fig. 2 A and B. Incubation of green-labeled LUVs with red-labeled GUVs led to progressive changes in the color of the GUV membrane due to lipid transfer of LUVs lipids to the GUV membrane (see the cartoon in Fig. S3). Thus, as a result of the increase in the extent of fusion as the LUV concentration increases, the GUVs exhibited three main colors: 1) red, 2) orange/yellow, and 3) green, related to no/low, intermediate, or high fusion efficiencies, respectively. The amount of fluorescent lipids transferred from fusogenic LUVs was quantified from the fluorescence intensity of DPPE-NBD on GUVs as a function of the fusogenic lipid concentration (Fig. 2 C and D).

In general, the LUV concentration-dependent behavior was similar for both binary compositions, and a progressive lipid transfer from LUVs was observed as the LUV concentration increased. This is seen from the images and more quantitatively from the green fluorescence intensity trans-

ferred to the GUVs. More specifically, for POPC:DPPG GUVs at low LUV concentrations (10 and 20  $\mu\text{M}$ ), LUVs docked predominantly onto the surface of the dark, negatively charged gel domains, where the LUVs are seen as diffraction-limited green dots (see white arrows in Fig. 2 A). Increased lipid concentrations (30  $\mu\text{M}$ ) resulted in significant fusion and a detectable increase in GUV area, where the GUVs were often no longer spherical because of acquiring excess surface area. In addition, the area of the dark (gel) domains decreased. At the highest LUV concentration (40  $\mu\text{M}$ ), a homogenous green signal was detected throughout the GUV surface, and the gel domains were completely dissolved because of the transfer of a large amount of fluid lipids from the fusogenic LUVs. At this stage, after so much fusion, the GUV regained a spherical shape and the excess area obtained from fusion with LUVs was stored in the form of buds and tubes. We have shown previously that this shape transition is caused by the increase in spontaneous curvature resulting from area leaflet asymmetry present in the LUVs that was transferred to the GUVs upon fusion (22). The images show that GUVs of both compositions become progressively yellow and then green and that the domains disappear. The results in Fig. 2 A are interesting and to some extent surprising, because they show that, although LUV docking occurs predominantly in the (negative) gel phase, membrane fusion is still very efficient, unlike interaction with charged and homogeneous gel GUVs.

In the case of POPG:DPPC GUVs (Fig. 2 B), changes in the domain shape and a more intense DPPE-NBD fluorescence signal on the GUV membrane were already observed after incubation with low lipid concentrations (20  $\mu\text{M}$ ). This is expected as, for this GUV composition, both LUV binding and fusion take place in the (negative) fluid phase. Furthermore, we did not observe docking, presumably due to the fast LUV fusion with negative fluid membranes, in the order of a few milliseconds (22). Further increasing LUV concentration (30  $\mu\text{M}$ ) also led to area increase that is stored in GUV budding. Note again that fusion is restricted to the outer membrane, and internal vesicles are not accessed by the LUVs (equatorial view in Fig. 2 B, 30  $\mu\text{M}$  lipids). The gel domains were already completely dissolved at 30  $\mu\text{M}$  LUVs and the DPPE-NBD dye was homogeneously distributed on the GUV surface. Similar outcomes were observed after GUVs were incubated for different periods of time with a fixed LUV concentration (15  $\mu\text{M}$  lipid) and then imaged (see Fig. S4): GUVs of both compositions become progressively yellow and then green and the domains disappear.

Quantification of the amount of green fluorescent probe transferred to the GUVs (Fig. 2 C and D) show that fusion efficiency is somewhat higher for the POPG:DPPC system, since higher transfer is observed for the intermediate fusogenic lipid concentrations (20 and 30  $\mu\text{M}$ ). However, both compositions show similarly high fusion efficiency for the highest fusogenic lipid concentration (40  $\mu\text{M}$ ).

Since efficient fusion was observed with both phase-separated systems, irrespective of the phase of the charged lipid, we have directly compared the fusion efficiency of these membrane compositions with that for the homogeneous fluid POPC:POPG investigated in detail previously (22) when incubated with an intermediate concentration of fusogenic lipids (25  $\mu\text{M}$ ). The amount of transferred lipid was quantified from the fluorescence intensity of the DPPE-NBD channel on the surface of the GUVs. Representative images of the GUVs after incubation and quantification of fluorescence transferred are shown in Fig. 3. Even though LUVs fused to all binary compositions investigated, statistically significant differences in fusion efficiency were observed. A somewhat higher fusion efficiency was detected for phase-separated POPG:DPPC as compared with homogeneous POPC:POPG. This indicates that phase separation can indeed enhance the fusion efficiency to the fluid negative portion, although mildly. On the other hand, lower fusion efficiency was detected for the POPC:DPPG system compared with the other two, but nonetheless higher than for the pure gel phase, for which no irrevocable sign of fusion was detected (see Fig. 1). It was also evident that

most of the POPG:DPPC vesicles ( $\sim 85\%$ ) were already homogeneous (homogeneous/phase-separated vesicles are shown as open/half-filled symbols in Fig. 3 B), in sharp contrast with POPC:DPPG vesicles, for which only a few did not exhibit phase separation ( $\sim 15\%$ ), showing again that less fusion has occurred when the negative lipid is in the gel phase.

#### Real-time membrane fusion using a flow chamber device

In the experiments above, we detected membrane fusion intermediates (docking and lipid mixing) as a function of LUV concentration after LUV-GUV incubation for a fixed period of time. Although the incubation approach offers the advantage that the GUVs are exposed to controlled and precise concentrations of LUVs for a given time and allow quantitative analysis of the fusion efficiency, one is only able to observe the final stage of a given process, whereas intermediate stages and the dynamics of the process are lost. Furthermore, characterization for phase state is practically performed over different vesicle populations. To observe membrane fusion in real time with fine spatio-temporal control of the interaction partners, we used a flow chamber to add LUVs to the GUVs in a controlled way. Using a flow chamber to trap GUVs or to study their dynamics has been proved to be a useful tool to observe changes in individual GUVs throughout the whole experiment (47–49), and a variation of this approach has been used by us to study membrane fusion with homogeneous charged membranes (22). We should stress, however, that even though this approach allows for time-resolved assessment of the complete fusion process on single vesicles, it does not permit detailed quantitative and comparative analysis of the fusion efficiency, as the actual concentration of LUVs reaching a specific GUV cannot be determined throughout the experiment, and absolute fluorescence intensity is affected by photobleaching, laser intensity, detector gain, vesicle size, etc.

Here, we injected LUVs to GUVs loaded in the channels of the flow chamber and followed the fusion-dependent changes in the GUVs. These changes can be followed at a single GUV level throughout the whole process, before and upon incubation with the LUVs and in real time. Each of the GUV binary compositions labeled with DPPE-Rh (red) were loaded in a flow chamber; the sugar asymmetry and subsequent sedimentation of the GUVs permitted the external solution to be exchanged without significantly displacing the GUVs. Fusogenic LUVs labeled with DPPE-NBD (green) and encapsulating 20  $\mu\text{M}$  ATTO 647 (gray) were introduced with a slow constant flow rate to facilitate imaging and minimize the displacement of the GUV on the coverslip. Although the precise concentration of LUVs reaching the GUVs cannot be determined because it depends on the position of each GUV in the flow chamber, we started observation when LUVs were detected close to the chosen GUV in the green or gray signal. Fig. 4 shows

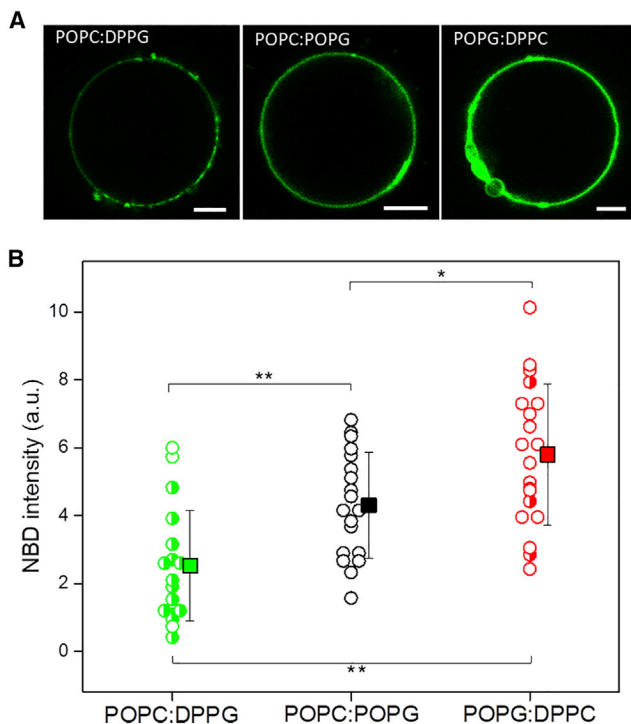
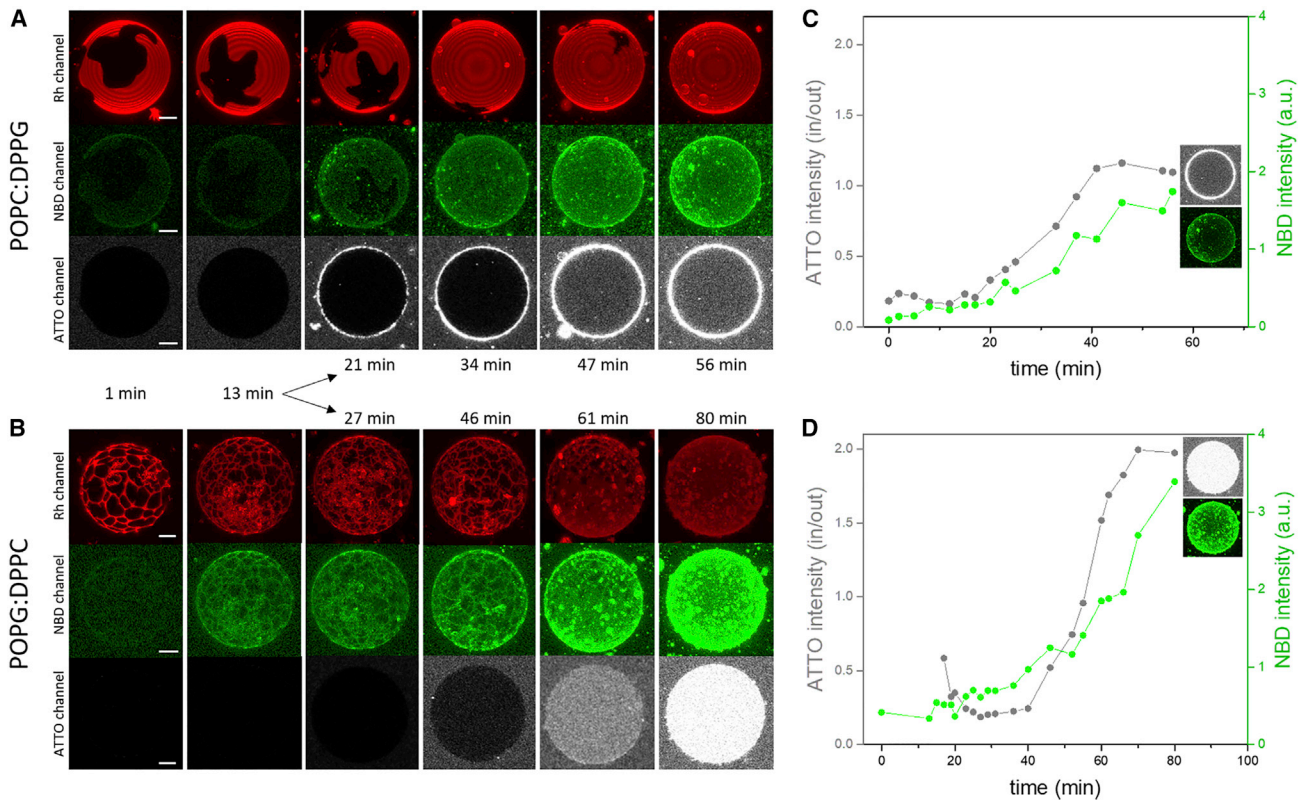


FIGURE 3 Quantification of DPPE-NBD transferred to GUVs of POPC:DPPG, POPC:POPG, and POPG:DPPC (1:1 mol:mol) upon fusion. (A) Confocal microscopy images of GUVs after incubation with LUVs of 25  $\mu\text{M}$  DOTAP:DOPE 1:1 with 1 mol % DPPE-NBD obtained in the DPPE-NBD (green) channel. Scale bars, 10  $\mu\text{m}$ . (B) Quantification of the DPPE-NBD fluorescence (in arbitrary units) transferred to the GUVs. Each symbol represents one vesicle, and mean values with SD are shown for each composition. Open symbols indicate homogeneous vesicles, whereas half-filled symbols represent phase-separated vesicles. \* $p < 0.05$ , \*\* $p < 0.01$  (one-way ANOVA Bonferroni test). To see this figure in color, go online.



**FIGURE 4** Single-vesicle fusion assay in a flow chamber shows that lipid mixing is coupled to content mixing. Representative confocal microscopy images of GUVs composed of (A) POPC:DPPG and (B) POPG:DPPC with 0.5 mol % DPPE-Rh during controlled addition of LUVs (210  $\mu$ M DOTAP:DOPE with 1 mol % DPPE-NBD and encapsulating 20  $\mu$ M ATTO 647) with a flow chamber. The time indicated is relative to the beginning of the recording, which was started as soon as the presence of the LUVs was detected in the green channel close to the selected GUV. Top rows, DPPE-Rh red channel (3D reconstruction of the bottom hemisphere); middle rows, DPPE-NBD green channel (3D reconstruction of the bottom hemisphere). The brightness (+40%) and contrast (-40%) of the green channel were modified to better visualize the beginning of the process; bottom rows, ATTO 647 gray channel (equatorial cross section). Scale bars, 10  $\mu$ m. (C) and (D) Graphs of the fluorescence intensity measured on the surface of the GUVs in the green channel (DPPE-NBD, in arbitrary units) and ratio between the ATTO 647 inside and outside the GUVs in the gray channel. For the former, line profiles across the equatorial slices were done and the intensity at the membrane was measured. The intensity values of the green channel were corrected for the laser intensity, which was different for the two compositions. To see this figure in color, go online.

the lower vesicle half in 3D projections of selected GUVs of each composition in the red and green (lipid mixing) channels and equatorial views in the gray (content mixing) channel as a function of time (see Fig. S5 for images of top hemispheres of each GUV composition). Overall, the sequences of images for both compositions showed that the dissolution of the domains (red channel) occurred simultaneously with the increase in the fluorescence signal from the fusogenic lipids (lipid mixing) on the surface of the GUVs (green channel). In other words, the dissolution of gel domains was coupled with membrane fusion. Lipid mixing was accompanied in the POPG:DPPC vesicle by content mixing, as seen by the concomitant increase in the ATTO 647 concentration (gray channel, Fig. 4 B). The graphs in Fig. 4 C and D show the progression of the fluorescence intensity of the green (in the membrane) and gray channels (ratio between the intensity inside and outside the GUV). The ATTO 647 signal shows a very efficient full fusion in the POPG:DPPC system, for which a higher intensity inside

the GUV was detected. On the other hand, the intensity of ATTO 647 inside the POPC:DPPG GUV became similar to that outside, saturating over time at in/out intensity ratio of 1, suggesting that this GUV became permeable around 40 min. Vesicle permeabilization was observed in several GUVs of both compositions after extensive fusion when phase contrast observation was employed (see Fig. S6, which shows that the percentage of GUVs with intact contrast due to sucrose/glucose asymmetry under phase contrast decreases with the fusogenic lipid concentration). Curiously, a very strong ATTO 647 signal was detected on the membrane of the POPC:DPPG vesicle, but not on POPG:DPPC. This might indicate a considerable quantity of adhered LUVs onto that system, even though extensive lipid mixing was detected as well.

The fusion processes of other GUVs were followed with the flow chamber and were found to exhibit the same overall behavior as in Fig. 4. The sequences and the quantification of the membrane and content mixing signals are shown in

**Fig. S7** for POPC:DPPG GUVs and **S8** for POPG:DPPC GUVs. All POPC:DPPG GUVs tracked became permeable (reached the same ATTO intensity inside and outside) and exhibited enhanced ATTO signal at the membrane surface (see **Fig. S7**). For the POPG:DPPC GUVs, clear content mixing was always detected (see **Fig. S8**). In all cases, fusion efficiency (increase in green fluorescence) was accompanied by domain dissolution. The absolute levels of transferred green fluorescence cannot be directly compared among all experiments/compositions, as different parameters (e.g., vesicle size and imaging location, different laser intensity, and detector gain settings optimized for the individual experiment) were used and photobleaching over long periods of illumination/observation had a direct effect on fluorescence intensity.

Altogether, real-time controlled experiments using flow chambers allowed us to follow qualitatively the transfer of lipids from the fusogenic liposomes into single GUVs and the dissolution of the domains that followed. Additionally, content mixing was detected concomitantly with the transfer of lipids for the POPG:DPPC system.

### Thermal behavior of lipid mixtures as seen by DSC

Fluorescence microscopy experiments showed that the incorporation of low- $T_m$  lipids via fusion from the LUVs led to the dissolution of the gel domains in the GUV membranes (leading from gel-fluid coexistence to predominantly fluid phase membrane). To investigate the thermal profile of the lipid mixtures and to gain insights into the suppression of phase separation and domain dissolution, DSC experi-

ments were performed. By observing the changes in the excess heat capacity ( $\Delta C_p$ ) with increasing the temperature, it is possible to assess the profile of the gel-fluid phase transition of a lipid bilayer (33) and determine the membrane phase of the investigated mixture at room temperature, the condition explored with microscopy. For these experiments, only LUVs were used since it is possible to control the lipid concentration and molar ratios of the fusogenic and acceptor mixtures.

It is well known that pure DPPC and DPPG have  $T_m$  around 41°C, so bilayers from these lipids are in the gel state at room temperature (33,50). On the other hand, the  $T_m$  of bilayers composed of POPC or POPG is -2°C, and membranes formed from these lipids are fluid at room temperature (34). Conversely, mixture of low- and high- $T_m$  lipids will usually result in a gel-fluid coexistence region in the phase diagram (51). Our DSC experiments show that LUVs composed of equimolar mixtures of POPC:DPPG and POPG:DPPC exhibit broad transition regions between 10°C and 30°C, and are therefore in the gel-fluid coexistence region at room temperature (**Fig. 5**, black curves). The thermal profiles of both mixtures are somewhat different. POPC:DPPG (**Fig. 5 A**) exhibits a broad transition between two bands, which is compatible with a well-phase-separated system, as observed with confocal microscopy (see **Figs. 2 A** and **S2 A**). On the other hand, POPG:DPPC (**Fig. 5 B**) shows a narrower profile, probably indicating a higher miscibility of the two lipids, which is probably reflected in the smaller size of the linear domains formed (see **Figs. 2 B** and **S2 B**). However, both mixtures are in the transition region at room temperature and become fluid at approximately 30°C.

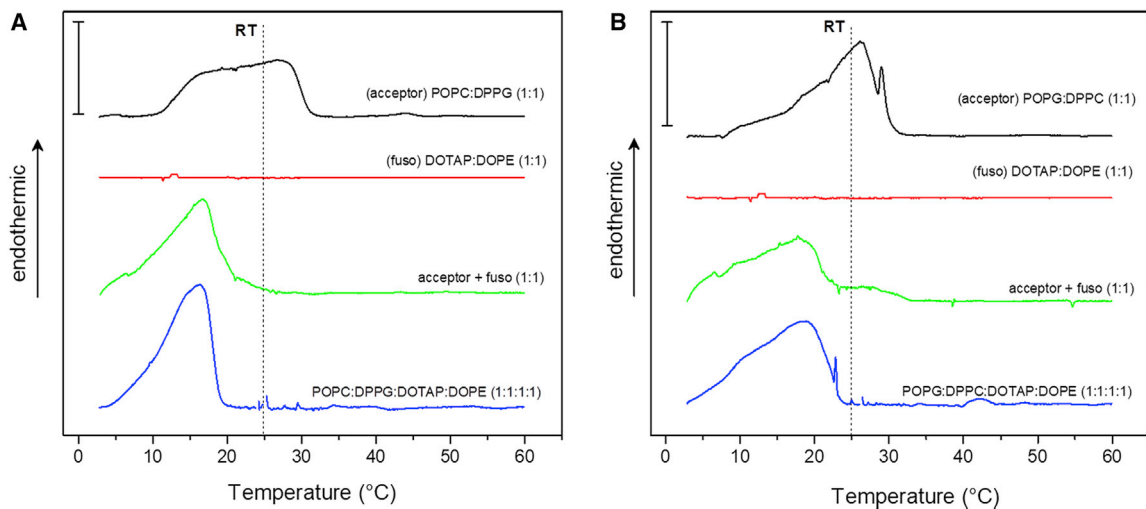


**FIGURE 5** DSC thermograms of LUVs. DSCs of the acceptor LUVs composed of 5 mM (A) POPC:DPPG (1:1) and (B) POPG:DPPC (1:1) before (black curves) and after (green curves) mixing with the fusogenic system (5 mM DOTAP:DOPE, 1:1; red curve) and of LUVs preformed from the full mixtures of each system (blue curves). The curves were vertically shifted for better visualization, and the room temperature (RT) is indicated with a vertical dashed line. The scale bars in the upper left corners indicate 1 kcal/mol/°C. The magnitude of  $\Delta C_p$  is given per mole of DPPC or DPPG in the mixture, since these are the only lipids that melt in this temperature range (the only exception is the fusogenic mixture, which is given per total mole of lipids). The scan rate was 20°C/h. To see this figure in color, go online.

DSC experiments were also performed on LUVs composed of the fusogenic system DOTAP:DOPE (1:1). The thermogram of this system (Fig. 5, red curve) shows that the equimolar mixture of the DOTAP:DOPE vesicles is fluid throughout the temperature scan, as expected, since the  $T_m$  values of these lipids are below 0°C (52,53).

Next, both binary compositions of the acceptor system were incubated for 20 min with the fusogenic system in a 1:1 acceptor:fuso molar ratio and DSC scans were then obtained (Fig. 5, green traces). The thermograms show that the transition region shifts to lower temperatures, as expected, and at room temperature both mixtures are in the fluid state. No clear differences were observed between the two acceptor systems. To assess the thermal behavior of fully mixed acceptor and fusogenic systems, LUVs were prepared containing equimolar mixtures of all lipids: POPC:DPPG:DOTAP:DOPE (1:1:1:1) and POPG:DPPC:DOTAP:DOPE (1:1:1:1) (Fig. 5, blue curves). Both compositions show a relatively high miscibility and a transition band around 15°C and are completely fluid above 22°C. Importantly, the thermal profiles of the acceptor:fuso 1:1 of both systems (green curves) are very similar to those of the fully mixed systems (blue curves), showing that fusion is extensive in both systems, corroborating the dissolution of the domains observed in the microscopy experiments for both compositions. The enthalpy variations of the transitions were around  $\Delta H \sim 9\text{--}10$  kcal per mole of DPPC or DPPG for all scans, in agreement with the enthalpy variations of pure DPPC and DPPG (33).

## DISCUSSION AND CONCLUSIONS

Membrane fusion is a fundamental process by which cells communicate with the environment and transduce intracellular signals. Although reconstituted systems lack the molecular complexity of fusion observed in living cells, in which both the extent and kinetics are shown to differ from those seen in live cells (54–56), they bypass the complexity of such processes by affording precise control of the membrane and environmental components while avoiding the influence of peripheral processes that are only marginally associated with fusion. Although we have recently characterized some of the molecular and mechanical aspects of fusion between oppositely charged LUVs and GUVs, these studies have been limited to the use of fluid and homogeneous membranes (22,23). Here we carried out a comprehensive study to also take into account the role of membrane phase state on membrane fusion. For that purpose, we first examined homogeneous membranes in different phase states (gel and fluid) and then phase separated membranes in which one of the domains was negatively charged. As expected, high fusion efficiency of cationic LUVs with single-component GUVs was restricted to POPG membranes (i.e., fluid and negative). Fusion with POPC was limited, whereas fusion with gel phase membranes was hindered regardless of charge, as a consequence

of the very high bending rigidity and resistance to shearing of gel phase membranes (22,57,58). Fusion efficiency was high in both phase-separated GUVs, when the negative lipid was in the fluid (POPG:DPPC) but also in the gel (POPC:DPPG) state, although slower and less efficient for the latter. In both systems, transfer of large amounts of low- $T_m$  lipids from the LUVs (DOTAP and DOPE) to the phase-separated GUVs eventually led to phase separation suppression and the dissolution of the gel domains. In fact, if fusion proceeds up to charge neutralization, as expected from our previous studies (22,23), then the final membrane composition consists of a fluid:gel lipid ratio of 3:1, hence leading to the reorganization of the lipid domains in the bilayer. Quite importantly, when the fusion efficiencies of the two phase-separated systems were compared with the homogeneous fluid system POPC:POPG explored in detail in our previous study (22), a mild but statistically significant increase in lipid mixing was observed when POPG was phase separated (POPG:DPPC versus POPC:POPG). Thus, our results show that phase separation increases the fusion efficiency.

As previously mentioned, multiple steps precede the final and efficient fusion between two opposing membranes. More specially, for the stalk formation, an energy barrier must be overcome so that the following steps can take place. For an efficient membrane fusion, a low energy barrier in the system is expected. Oppositely charged membranes attract each other, and that facilitates a tight contact. Then, phase separation can facilitate fusion, since simulations have previously shown that, near the boundaries of phase-separated membranes, the asymmetry causes the relaxation of the deformation energy, which decreases energy barriers and facilitates fusion (59). The fact that POPG:DPPG exhibited more lipid mixing than POPC:POPG and that such a high fusion efficiency was detected also in the POPC:DPPG system indicates that phase separation and presence of domain boundaries in our experiments also favor membrane fusion. The shape of the domains in the POPG:DPPC could also favor more efficient fusion, as a much higher fraction of domain boundaries exist for this composition. In addition, bilayer thickness mismatch can lead to the formation of “soft” boundary regions throughout the membrane. Therefore, fusion with DPPG lipids might start in the vicinity of the domain boundaries, where such lipids might be more disordered, or with the few DPPG lipids present in the fluid domains. This rationale would be consistent with the fact that fusion is slower in the POPC:DPPG system, but almost as effective as with the POPG:DPPC membranes for higher fusogenic lipid concentration.

The fact that phase separation can facilitate fusion can have clear physiological implications, as biomembranes are highly heterogeneous, not only due to the existence of membrane rafts, which are supposed to be close to the liquid-ordered phase, but also to the highly heterogeneous

distribution of proteins and the presence of the cytoskeleton on the leaflet facing the cytosol. The results presented here are relevant not only in the field of biophysics but also in cell biology, as the reorganization of lipid domains in the cell membrane can affect a wide range of biological processes. Membrane organization can either promote cell viability, such as cell proliferation and adhesion, or allow viral and bacterial infection (27,60–63). The presence of lipid charged domains in bacteria have been proposed to exist and to influence protein ordering within the membrane (64). Targeting anionic lipids in the lipid domains can be used to deliver antimicrobial agents, for instance. Moreover, the mechanism of how  $\text{Ca}^{2+}$  can trigger membrane fusion involves inducing phase separation in cells. More specifically, this mechanism has been associated with its capacity to induce the formation of phase boundaries as a result of molecular packing (65,66). Our group is now investigating how to controllably induce phase separation in the acceptor membrane using a novel highly fusogenic system composition. Thus, understanding molecular details of how phase separation can be controlled has an important role in maintaining cell viability and investigating possible mechanism of actions of promising drug molecules.

In summary, we have extended the use of GUVs as a model system for membrane fusion investigations where the effects of both charge, phase state, and phase separation on fusion efficiency were directly visualized by a combination of optical imaging and thermal analysis using DSC. By tuning membrane charges, we could control the preferential binding sites of cationic fusogenic LUVs and, to some extent, the location of fusion events. The results show that both membrane charges as well as the membrane phase state control the ability of cationic fusogenic LUVs to fuse with acceptor membranes. Of note, phase separation favors membrane fusion irrespective of the domain charge. Efficient fusion results in a high transfer of lipids to the acceptor membranes, leading to a complete restructuring of membrane organization. More generally, the study sheds light on the modes of interaction of cationic fusogenic liposomes with heterogeneous membranes and could potentially be extended to cells. More specifically, it highlights the importance of understanding complex cargo-carrier mechanical effects in cells during intracellular delivery. Efficient fusogenic liposomes thus have the potential to bypass slow and inefficient internalization pathways and could deliver intracellularly a large range of materials that would become readily available, while offsetting the possible side effects associated with cell interactions, both of which are major goals in the field of drug delivery.

## SUPPORTING MATERIAL

Supporting material can be found online at <https://doi.org/10.1016/j.bpj.2022.12.008>.

## AUTHOR CONTRIBUTIONS

K.A.R., R.D., and R.B.L. conceived the study and designed the experiments. R.R.M.C. performed the experiments and analyzed the data. E.J.E. contributed to the experiments using the flow chamber. The manuscript was written by all authors.

## ACKNOWLEDGMENTS

The financial supports of FAPESP (2016/13368-4, 2017/9367-5, 2018/08014-4) and CNPq are acknowledged.

## DECLARATION OF INTERESTS

The authors declare no competing interests.

## REFERENCES

- Rand, R. P., and V. A. Parsegian. 1986. Mimicry and mechanism in phospholipid models of membrane fusion. *Annu. Rev. Physiol.* 48:201–212. <https://doi.org/10.1146/annurev.ph.48.030186.001221>.
- Jahn, R., T. Lang, and T. C. Südhof. 2003. Membrane fusion. *Cell.* 112:519–533. [https://doi.org/10.1016/s0092-8674\(03\)00112-0](https://doi.org/10.1016/s0092-8674(03)00112-0).
- Harrison, S. C. 2008. Viral membrane fusion. *Nat. Struct. Mol. Biol.* 15:690–698. <https://doi.org/10.1038/nsmb.1456>.
- Petrany, M. J., and D. P. Millay. 2019. Cell fusion: merging membranes and making muscle. *Trends Cell Biol.* 29:964–973. <https://doi.org/10.1016/j.tcb.2019.09.002>.
- Boonstra, S., J. S. Blijleven, ..., A. M. van Oijen. 2018. Hemagglutinin-mediated membrane fusion: a biophysical perspective. *Annu. Rev. Biophys.* 47:153–173. <https://doi.org/10.1146/annurev-biophys-070317-033018>.
- Barrett, C. T., and R. E. Dutch. 2020. Viral membrane fusion and the transmembrane domain. *Viruses.* 12:693. <https://doi.org/10.3390/v12070693>.
- Martens, S., and H. T. McMahon. 2008. Mechanisms of membrane fusion: disparate players and common principles. *Nat. Rev. Mol. Cell Biol.* 9:543–556. <https://doi.org/10.1038/nrm2417>.
- Chernomordik, L. V., and M. M. Kozlov. 2008. Mechanics of membrane fusion. *Nat. Struct. Mol. Biol.* 15:675–683. <https://doi.org/10.1038/nsmb.145>.
- Nickel, W., T. Weber, ..., J. E. Rothman. 1999. Content mixing and membrane integrity during membrane fusion driven by pairing of isolated v-SNAREs and t-SNAREs. *Proc. Natl. Acad. Sci. USA.* 96:12571–12576. <https://doi.org/10.1073/pnas.96.22.12571>.
- Peetla, C., K. S. Rao, and V. Labhasetwar. 2009. Relevance of biophysical interactions of nanoparticles with a model membrane in predicting cellular uptake: study with TAT peptide-conjugated nanoparticles. *Mol. Pharm.* 6:1311–1320. <https://doi.org/10.1021/mp900011h>.
- Sercombe, L., T. Veerati, ..., S. Hua. 2015. Advances and challenges of liposome assisted drug delivery. *Front. Pharmacol.* 6:286. <https://doi.org/10.3389/fphar.2015.00286>.
- Friend, D. S., D. Papahadjopoulos, and R. J. Debs. 1996. Endocytosis and intracellular processing accompanying transfection mediated by cationic liposomes. *Biochim. Biophys. Acta.* 1278:41–50. [https://doi.org/10.1016/0005-2736\(95\)00219-7](https://doi.org/10.1016/0005-2736(95)00219-7).
- Wasungu, L., and D. Hoekstra. 2006. Cationic lipids, lipoplexes and intracellular delivery of genes. *J. Control. Release.* 116:255–264. <https://doi.org/10.1016/j.jconrel.2006.06.024>.
- Degors, I. M. S., C. Wang, ..., I. S. Zuhorn. 2019. Carriers break barriers in drug delivery: endocytosis and endosomal escape of gene delivery vectors. *Acc. Chem. Res.* 52:1750–1760. <https://doi.org/10.1021/acs.accounts.9b00177>.

15. Csiszár, A., N. Hersch, ..., B. Hoffmann. 2010. Novel fusogenic liposomes for fluorescent cell labeling and membrane modification. *Bioconj. Chem.* 21:537–543. <https://doi.org/10.1021/bc900470y>.
16. Kleusch, C., N. Hersch, ..., A. Csiszár. 2012. Fluorescent lipids: functional parts of fusogenic liposomes and tools for cell membrane labeling and visualization. *Molecules.* 17:1055–1073. <https://doi.org/10.3390/molecules17011055>.
17. Kube, S., N. Hersch, ..., A. Csiszár. 2017. Fusogenic liposomes as nanocarriers for the delivery of intracellular proteins. *Langmuir.* 33:1051–1059. <https://doi.org/10.1021/acs.langmuir.6b04304>.
18. Lira, R. B., M. A. B. L. Seabra, ..., A. Fontes. 2013. Studies on intracellular delivery of carboxyl-coated CdTe quantum dots mediated by fusogenic liposomes. *J. Mater. Chem. B.* 1:4297–4305. <https://doi.org/10.1039/c3tb20245c>.
19. Südhof, T. C. 2013. Neurotransmitter release: the last millisecond in the life of a synaptic vesicle. *Neuron.* 80:675–690. <https://doi.org/10.1016/j.neuron.2013.10.022>.
20. Rizzoli, S. O. 2014. Synaptic vesicle recycling: steps and principles. *EMBO J.* 33:788–822. <https://doi.org/10.1002/embj.201386357>.
21. Lira, R. B., and R. Dimova. 2019. Chapter six: fusion assays for model membranes. *Advances in Biomembranes and Lipid Self-Assembly.* Elsevier. <https://doi.org/10.1016/bs.abl.2019.09.003>.
22. Lira, R. B., T. Robinson, ..., K. A. Riske. 2019. Highly efficient protein-free membrane fusion: a giant vesicle study. *Biophys. J.* 116:79–91. <https://doi.org/10.1016/j.bpj.2018.11.3128>.
23. Cavalcanti, R. R. M., R. B. Lira, and K. A. Riske. 2022. Membrane fusion biophysical analysis of fusogenic liposomes. *Langmuir.* 38:10430–10441. <https://doi.org/10.1021/acs.langmuir.2c01169>.
24. Tilcock, C. P. S., and P. R. Cullis. 1982. The polymorphic phase behaviour and miscibility properties of synthetic phosphatidylethanolamines. *Biochim. Biophys. Acta Biomembr.* 684:212–218. [https://doi.org/10.1016/0005-2736\(82\)90008-6](https://doi.org/10.1016/0005-2736(82)90008-6).
25. Jacobson, K., O. G. Mouritsen, and R. G. W. Anderson. 2007. Lipid rafts: at a crossroad between cell biology and physics. *Nat. Cell Biol.* 9:7–14. <https://doi.org/10.1038/ncb0107-7>.
26. Kasson, P., and V. S. Pande. 2007. Control of membrane fusion mechanism by lipid composition: predictions from ensemble molecular dynamics. *PLoS Comput. Biol.* e220 <https://doi.org/10.1371/journal.pcbi.0030220>.
27. van Meer, G., D. R. Voelker, and G. W. Feigenson. 2008. Membrane lipids: where they are and how they behave. *Nat. Rev. Mol. Cell Biol.* 9:112–124. <https://doi.org/10.1038/nrm2330>.
28. Lingwood, D., and K. Simons. 2010. Lipid rafts as a membrane-organizing principle. *Science.* 327:46–50. <https://doi.org/10.1126/science.1174621>.
29. Holthuis, J. C. M., and A. K. Menon. 2014. Lipid landscapes and pipelines in membrane homeostasis. *Nature.* 510:48–57. <https://doi.org/10.1038/nature13474>.
30. Ahmed, S. N., D. A. Brown, and E. London. 1997. On the Origin of sphingolipid/cholesterol-rich detergent-insoluble cell membranes: physiological concentrations of cholesterol and sphingolipid induce formation of a detergent-insoluble, liquid-ordered lipid phase in model membranes. *Biochemistry.* 36:10944–10953. <https://doi.org/10.1021/bi971167g>.
31. McMullen, T. P., R. N. Lewis, and R. N. McElhaney. 2004. Cholesterol–phospholipid interactions, the liquid-ordered phase and lipid rafts in model and biological membranes. *Curr. Opin. Colloid Interface Sci.* 8:459–468. <https://doi.org/10.1016/j.cocis.2004.01.007>.
32. Cevc, G. 1991. How membrane chain-melting phase-transition temperature is affected by the lipid chain asymmetry and degree of unsaturation: an effective chain-length model. *Biochemistry.* 30:7186–7193. <https://doi.org/10.1021/bi00243a021>.
33. Riske, K. A., R. P. Barroso, ..., M. T. Lamy. 2009. Lipid bilayer pre-transition as the beginning of the melting process. *Biochim. Biophys. Acta.* 1788:954–963. <https://doi.org/10.1016/j.bbmem.2009.01.007>.
34. Veatch, S. L., and S. L. Keller. 2003. Separation of liquid phases in giant vesicles of ternary mixtures of phospholipids and cholesterol. *Biophys. J.* 85:3074–3083. [https://doi.org/10.1016/s0006-3495\(03\)74726-2](https://doi.org/10.1016/s0006-3495(03)74726-2).
35. Yeagle, P. L. 2004. *The Structure of Biological Membranes.* CRC Press. <https://doi.org/10.1201/9781420040203>.
36. Quinn, P. J. 2010. A lipid matrix model of membrane raft structure. *Prog. Lipid Res.* 49:390–406. <https://doi.org/10.1016/j.plipres.2010.05.002>.
37. Imam, Z. I., L. E. Kenyon, ..., J. C. Stachowiak. 2017. Phase-separated liposomes enhance the efficiency of macromolecular delivery to the cellular cytoplasm. *Cell. Mol. Bioeng.* 10:387–403. <https://doi.org/10.1007/s12195-017-0489-4>.
38. Trementozzi, A. N., Z. I. Imam, ..., J. C. Stachowiak. 2019. Liposome-mediated chemotherapeutic delivery is synergistically enhanced by ternary lipid compositions and cationic lipids. *Langmuir.* 35:12532–12542. <https://doi.org/10.1021/acs.langmuir.9b01965>.
39. Yang, S.-T., V. Kiessling, ..., L. K. Tamm. 2015. HIV gp41-mediated membrane fusion occurs at edges of cholesterol-rich lipid domains. *Nat. Chem. Biol.* 11:424–431. <https://doi.org/10.1038/nchembio.1800>.
40. Yang, S.-T., A. J. B. Kreutzberger, ..., L. K. Tamm. 2017. HIV virions sense plasma membrane heterogeneity for cell entry. *Sci. Adv.* 3:e1700338. <https://doi.org/10.1126/sciadv.1700338>.
41. Hope, M. J., M. B. Bally, ..., P. R. Cullis. 1986. Generation of multilamellar and unilamellar phospholipid vesicles. *Chem. Phys. Lipids.* 40:89–107. [https://doi.org/10.1016/0009-3084\(86\)90065-4](https://doi.org/10.1016/0009-3084(86)90065-4).
42. Mesquita, R. M., E. Melo, ..., W. L. Vaz. 2000. Partitioning of amphiphiles between coexisting ordered and disordered phases in two-phase lipid bilayer membranes. *Biophys. J.* 78:3019–3025. [https://doi.org/10.1016/s0006-3495\(00\)76840-8](https://doi.org/10.1016/s0006-3495(00)76840-8).
43. Weng, C.-J., J.-P. Wu, ..., Y.-W. Hsueh. 2016. The influence of NBD fluorescent probe on model membranes containing POPC and DPPC. *Mol. Membr. Biol.* 33:23–28. <https://doi.org/10.1080/09687688.2016.1185175>.
44. Himeno, H., N. Shimokawa, ..., M. Takagi. 2014. Charge-induced phase separation in lipid membranes. *Soft Matter.* 10:7959–7967. <https://doi.org/10.1039/c4sm01089b>.
45. Bagatolli, L. A., and E. Gratton. 2000. A correlation between lipid domain shape and binary phospholipid mixture composition in free standing bilayers: a two-photon fluorescence microscopy study. *Biophys. J.* 79:434–447. [https://doi.org/10.1016/s0006-3495\(00\)76305-3](https://doi.org/10.1016/s0006-3495(00)76305-3).
46. Sharma, P., D. Singh, ..., A. Kanga. 2018. Are we neglecting nontuberculous mycobacteria just as laboratory contaminants? Time to reevaluate things. *J. Pathog.* 2018, 8907629. <https://doi.org/10.1155/2018/8907629>.
47. Nagle, J. F., and H. L. Scott. 1978. Lateral compressibility of lipid mono- and bilayers. Theory of membrane permeability. *Biochim. Biophys. Acta.* 513:236–243. [https://doi.org/10.1016/0005-2736\(78\)90176-1](https://doi.org/10.1016/0005-2736(78)90176-1).
48. Robinson, T., P. Kuhn, ..., P. S. Dittich. 2013. Microfluidic trapping of giant unilamellar vesicles to study transport through a membrane pore. *Biomicrofluidics.* 7:44105. <https://doi.org/10.1063/1.4816712>.
49. Robinson, T. 2019. Microfluidic handling and analysis of giant vesicles for use as artificial cells: a review. *Adv. Biosyst.* 3, 1800318. <https://doi.org/10.1002/adbi.201800318>.
50. McElhaney, R. N. 1982. The use of differential scanning calorimetry and differential thermal analysis in studies of model and biological membranes. *Chem. Phys. Lipids.* 30:229–259. [https://doi.org/10.1016/0009-3084\(82\)90053-6](https://doi.org/10.1016/0009-3084(82)90053-6).
51. Svetlovics, J. A., S. A. Wheaton, and P. F. Almeida. 2012. Phase separation and fluctuations in mixtures of a saturated and an unsaturated phospholipid. *Biophys. J.* 102:2526–2535. <https://doi.org/10.1016/j.bpj.2012.04.017>.
52. Koynova, R., and M. Caffrey. 1994. Phases and phase transitions of the hydrated phosphatidylethanolamines. *Chem. Phys. Lipids.* 69:1–34. [https://doi.org/10.1016/0009-3084\(94\)90024-8](https://doi.org/10.1016/0009-3084(94)90024-8).

53. Koynova, R., and M. Caffrey. 1998. Phases and phase transitions of the phosphatidylcholines. *Biochim. Biophys. Acta.* 1376:91–145. [https://doi.org/10.1016/s0304-4157\(98\)00006-9](https://doi.org/10.1016/s0304-4157(98)00006-9).
54. Mills, J. K., and D. Needham. 2005. Lysolipid incorporation in dipalmitoylphosphatidylcholine bilayer membranes enhances the ion permeability and drug release rates at the membrane phase transition. *Biochim. Biophys. Acta.* 1716:77–96. <https://doi.org/10.1016/j.bbame.2005.08.007>.
55. Lira, R. B., J. Steinkühler, ..., K. A. Riske. 2016. Posing for a picture: vesicle immobilization in agarose gel. *Sci. Rep.* 6:25254. <https://doi.org/10.1038/srep25254>.
56. Knorr, R. L., J. Steinkühler, and R. Dimova. 2018. Micron-sized domains in quasi single-component giant vesicles. *Biochim. Biophys. Acta Biomembr.* 1860:1957–1964. <https://doi.org/10.1016/j.bbame.2018.06.015>.
57. Fernandez-Puente, L., I. Bivas, ..., P. Méléard. 1994. Temperature and chain length effects on bending elasticity of phosphatidylcholine bilayers. *Europhys. Lett.* 28:181–186. <https://doi.org/10.1209/0295-5075/28/3/005>.
58. Dimova, R. 2014. Recent developments in the field of bending rigidity measurements on membranes. *Adv. Colloid Interface Sci.* 208:225–234. <https://doi.org/10.1016/j.cis.2014.03.003>.
59. Molotkovsky, R. J., V. V. Alexandrova, ..., S. A. Akimov. 2018. Lateral membrane heterogeneity regulates viral-induced membrane fusion during HIV entry. *Int. J. Mol. Sci.* 19:1483. <https://doi.org/10.3390/ijms19051483>.
60. Wymann, M. P., and R. Schneter. 2008. Lipid signalling in disease. *Nat. Rev. Mol. Cell Biol.* 9:162–176. <https://doi.org/10.1038/nrm2335>.
61. Ewers, H., and A. Helenius. 2011. Lipid-mediated endocytosis. *Cold Spring Harb. Perspect. Biol.* 3, a004721. <https://doi.org/10.1101/cshperspect.a004721>.
62. Lorizate, M., and H. G. Kräusslich. 2011. Role of lipids in virus replication. *Cold Spring Harb. Perspect. Biol.* 3:a004820. <https://doi.org/10.1101/cshperspect.a004820>.
63. Mahadeo, M., S. Nathoo, ..., E. J. Prenner. 2015. Disruption of lipid domain organization in monolayers of complex yeast lipid extracts induced by the lysophosphatidylcholine analogue edelfosine in vivo. *Chem. Phys. Lipids.* 191:153–162. <https://doi.org/10.1016/j.chemphyslip.2015.09.004>.
64. Epanand, R. M., and R. F. Epanand. 2009. Domains in bacterial membranes and the action of antimicrobial agents. *Mol. Biosyst.* 5:580–587. <https://doi.org/10.1039/b900278m>.
65. Papahadjopoulos, D., W. J. Vail, ..., R. Lazo. 1977. Studies on membrane fusion. III. The role of calcium-induced phase changes. *Biochim. Biophys. Acta.* 465:579–598. [https://doi.org/10.1016/0005-2736\(77\)90275-9](https://doi.org/10.1016/0005-2736(77)90275-9).
66. Hoekstra, D. 1982. Role of lipid phase separations and membrane hydration in phospholipid vesicle fusion. *Biochemistry.* 21:2833–2840. <https://doi.org/10.1021/bi00541a004>.

**Biophysical Journal, Volume 122**

**Supplemental information**

**Efficient liposome fusion to phase-separated giant vesicles**

**Rafaela R.M. Cavalcanti, Rafael B. Lira, Eleanor J. Ewins, Rumiana Dimova, and Karin A. Riske**

## Efficient liposome fusion to phase-separated giant vesicles

*Rafaela R. M. Cavalcanti, Rafael B. Lira, Eleanor J. Ewins,  
Rumiana Dimova, Karin A. Riske*

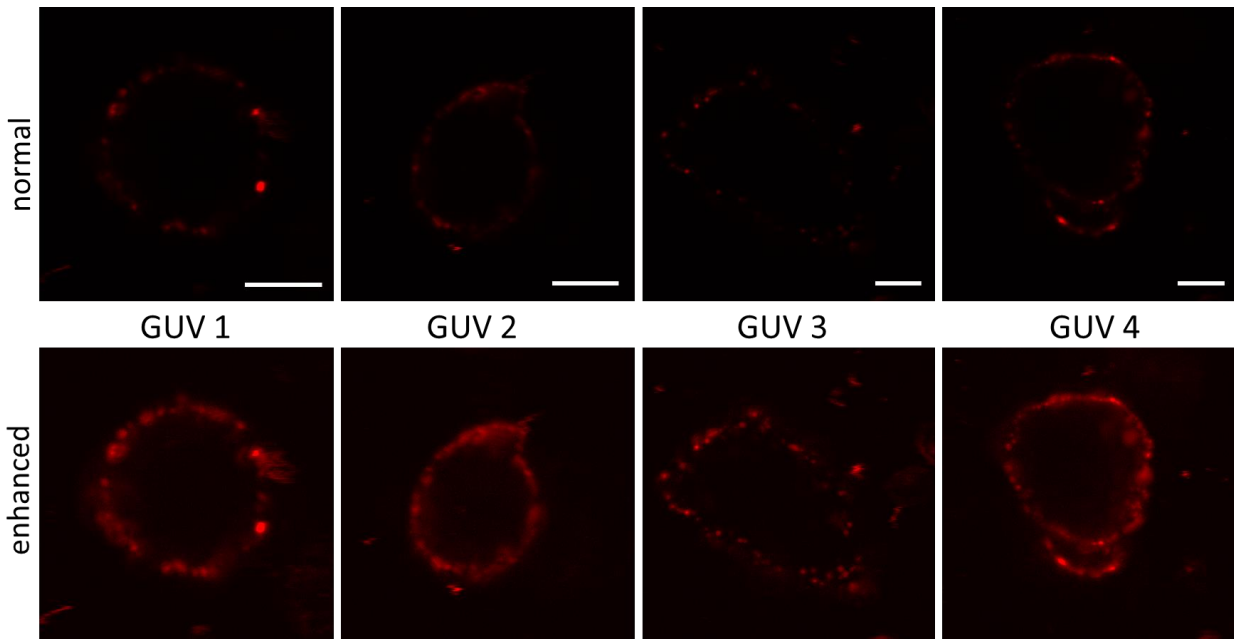


**Figure S1.** Confocal microscopy images of four DPPG GUVs containing 0.5 mol% DPPE-NBD after 15 minutes incubation with fusogenic LUVs (20  $\mu$ M DOTAP:DOPE with 1 mol% DPPE-Rh) acquired in the DPPE-Rh channel (excitation and emission set for DPPE-Rh detection). The images on the bottom are the same as on top but with contrast enhanced (+40 brightness/-40 contrast). Scale bars represent 5  $\mu$ m. GUV 1 is the same shown in Figure 1A.

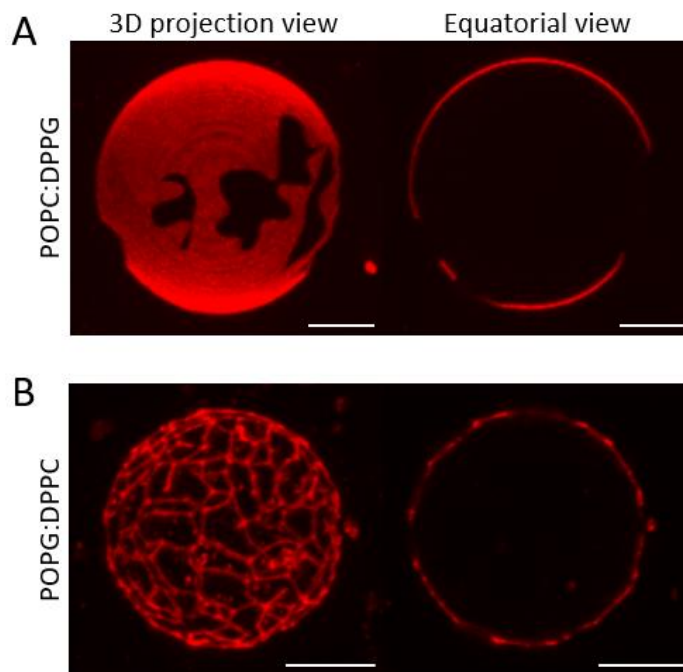


**Figure S2.** Representative confocal microscopy images of phase-separated GUVs composed of (A) POPC:DPPG (1:1) and (B) POPG:DPPC (1:1) labeled with 0.5 mol% DPPE-Rh in 3D projections of the GUV (left) and equatorial GUV sections (right). Scale bars: 10  $\mu\text{m}$ .

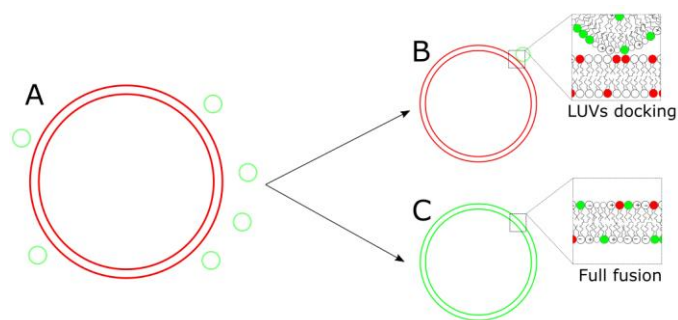


**Figure S3.** Cartoon showing fusion events between green-labeled (DPPE-NDB) LUVs and red-labeled (DPPE-Rh) GUVs. Incubation of LUVs and GUVs (A) can lead to docking of LUVs onto the GUV surface (B) or eventually to full fusion (C). The vesicles are not drawn to scale. The colors represent intensity changes due to lipid transfer.

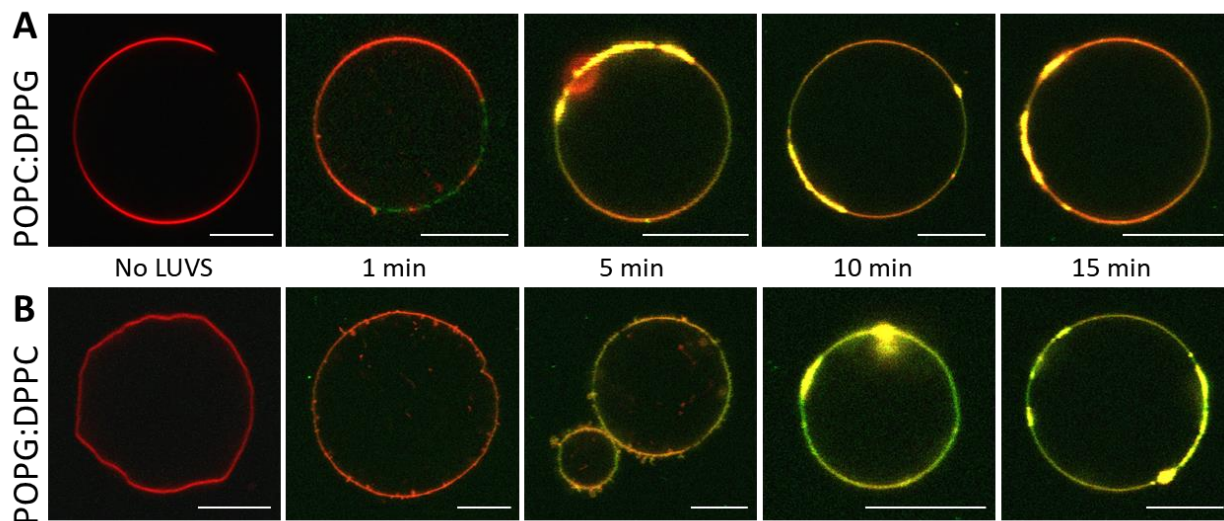


**Figure S4.** Overlay of DPPE-NBD and DPPE-Rh channels (equatorial sections) obtained with confocal microscopy of phase-separated GUVs composed of (A) POPC:DPPG and (B) POPG:DPPC with 0.5 mol% DPPE-Rh after incubation with fusogenic LUVs (15 μM, DOTAP:DOPE with 1 mol% DPPE-NBD). The time stamps indicate the incubation time. These images are from different GUVs in different incubation times. Scale bars: 10 μm.

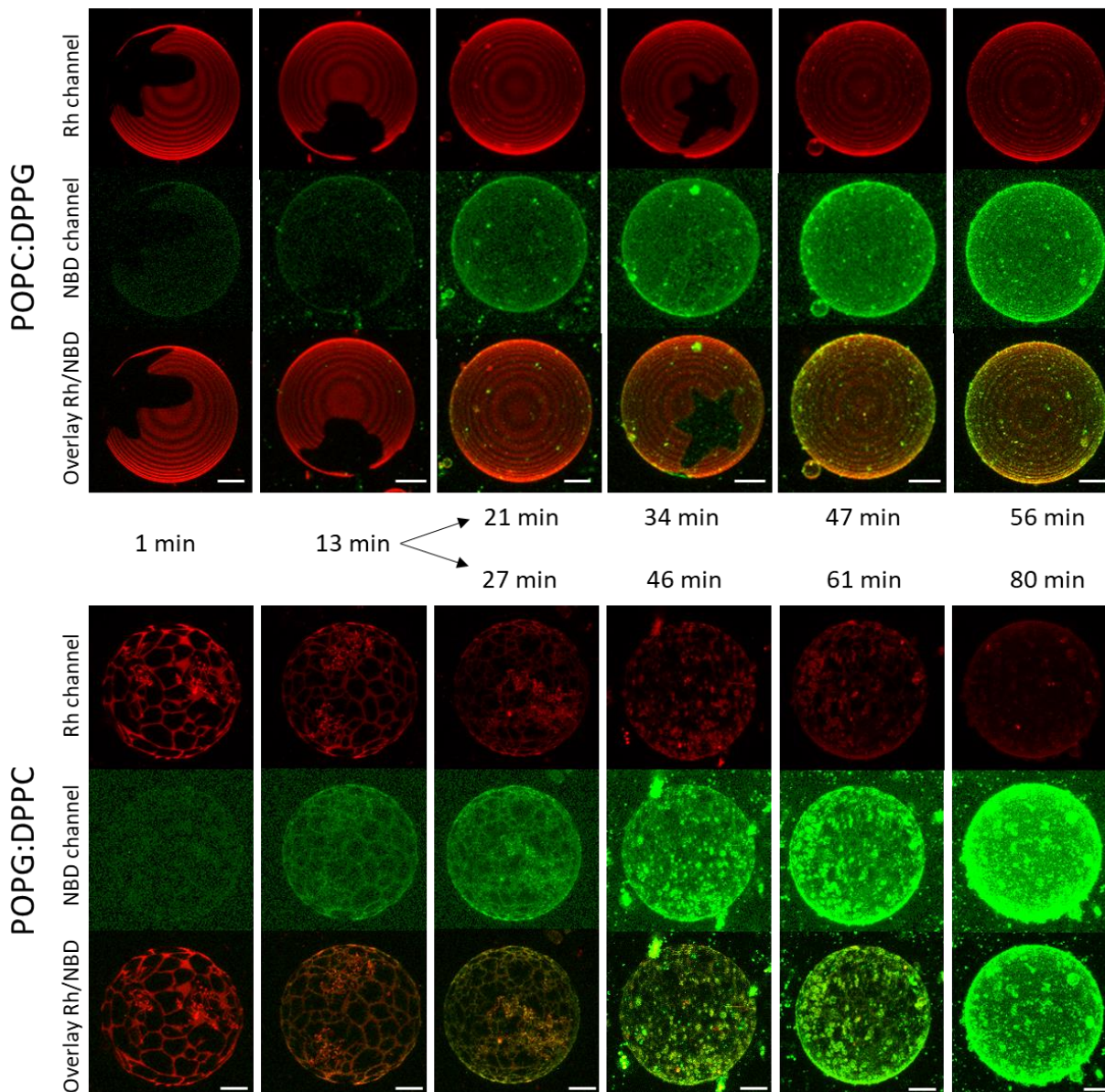


**Figure S5.** 3D reconstruction of confocal microscopy images of the top halves of GUVs composed of POPC:DPPG (1:1) and POPG:DPPC (1:1) with 0.5 mol% DPPE-Rh during controlled addition of LUVs (210  $\mu\text{M}$  DOTAP:DOPE, 1:1, with 1 mol% DPPE-NBD encapsulating 20  $\mu\text{M}$  ATTO 647) in a controlled flow chamber. The time indicated is relative to the beginning of the recording, which was started as soon as the presence of the LUVs was detected close to the selected GUV. The brightness (+ 40%) and contrast (- 40%) of the green channel were modified to better visualize the beginning of the process. Scale bars: 10  $\mu\text{m}$ . Scale bars: 10  $\mu\text{m}$ .

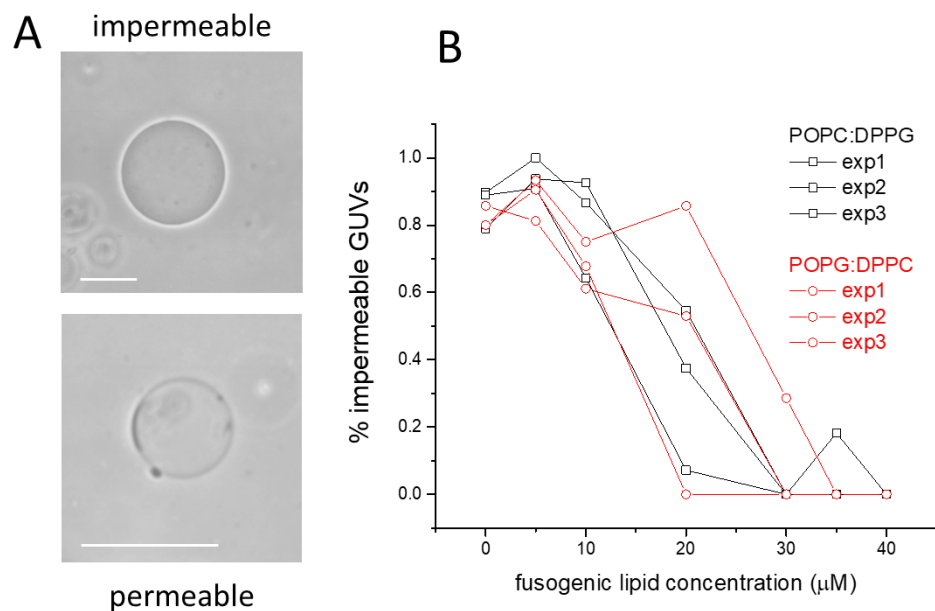


**Figure S6.** Quantification of permeabilized GUVs composed of POPC:DPPG POPG:DPPC (1:1). The GUVs were incubated with increasing concentrations of fusogenic lipids (DOTAP:DOPE 1:1) and were then observed under phase contrast microscopy in three separate experiments. (A) Phase contrast microscopy images of GUV with (top) and without (bottom) high optical contrast, identified as impermeable and permeable, respectively. Scale bars represent 10  $\mu\text{m}$ . (B) Fraction of impermeable GUVs (with high optical contrast) as function of the fusogenic lipids concentration for each experiment separately.

POPC:DPPG

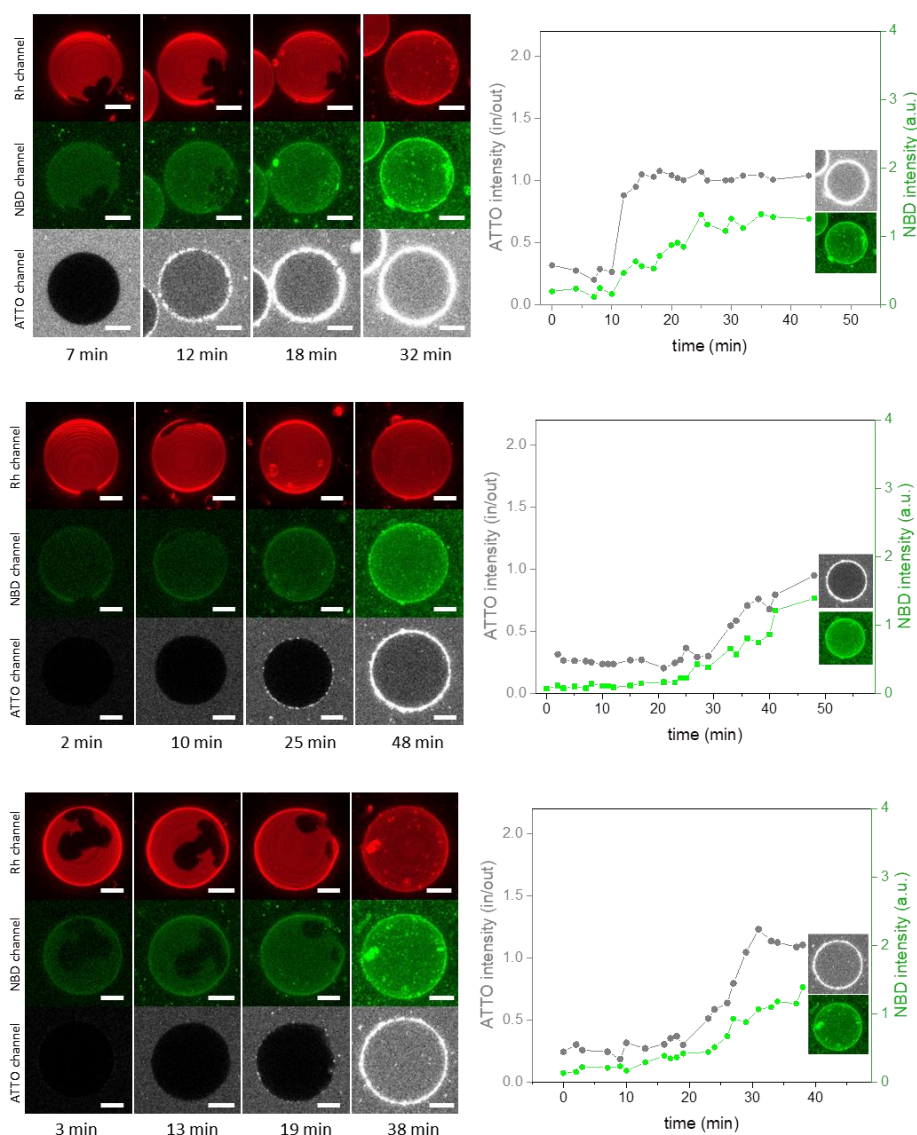


**Figure S7.** Single-vesicle fusion experiments in a flow chamber for GUVs composed of POPC:DPPG (1:1). Left panels: confocal microscopy images of three different GUVs composed of POPC:DPPG (1:1) with 0.5 mol% DPPE-Rh during controlled addition of LUVs (210  $\mu$ M DOTAP:DOPE with 1 mol% DPPE-NBD and encapsulating 20  $\mu$ M ATTO 647). The time indicated is relative to the beginning of the recording, which was started as soon as the presence of the LUVs was detected in the green channel close to the selected GUV. Top rows: DPPE-Rh red channel (3D reconstruction of the GUV bottom half); middle rows: DPPE-NBD green channel (3D reconstruction of the bottom half); bottom rows: ATTO 647 grey channel (equatorial cross section). Scale bars: 10  $\mu$ m. Right panels: Graphs of the fluorescence intensity measured on the surface of the GUVs in the green channel (DPPE-NBD) and ratio between the ATTO 647 intensity inside and outside the GUVs in the grey channel. The analyses were performed as described in Fig. 4 in the main text. The brightness (+ 40%) and contrast (- 40%) of the green and red channels were modified to better visualize the beginning of the process.

POPG:DPPC

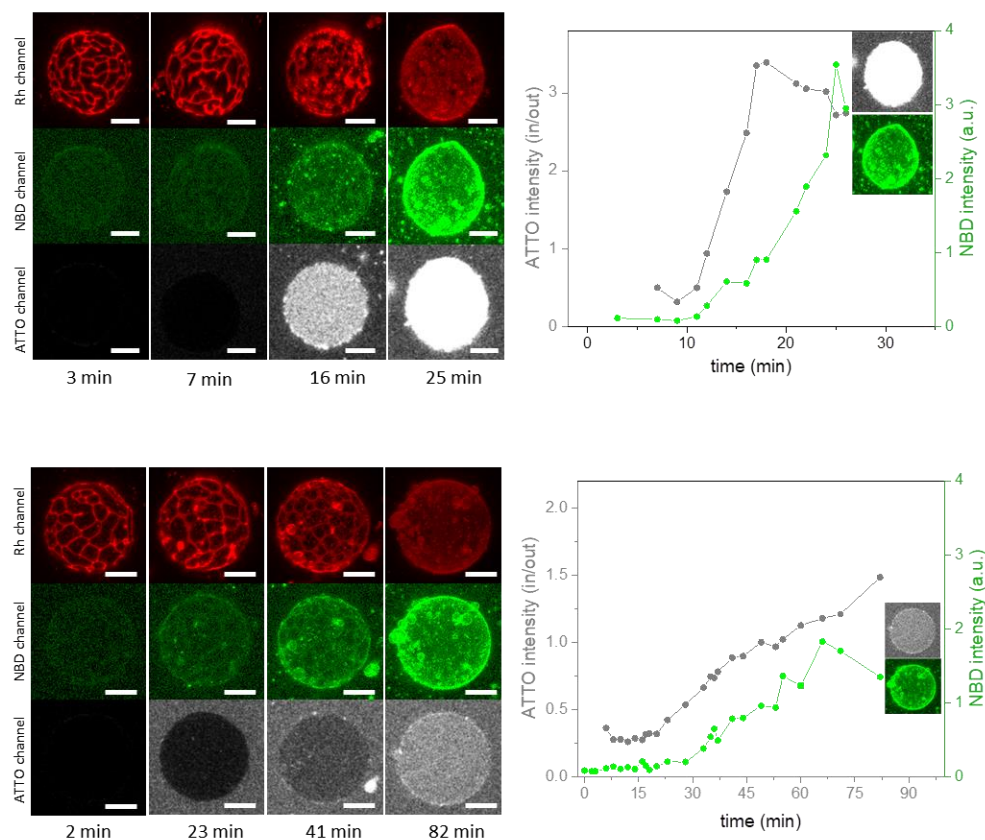


**Figure S8.** Single-vesicle fusion experiments in a flow chamber for GUVs composed of POPG:DPPC (1:1). Left panels: confocal microscopy images of two different GUVs composed of POPG:DPPC (1:1) with 0.5 mol% DPPE-Rh during controlled addition of LUVs (210  $\mu$ M DOTAP:DOPE with 1 mol% DPPE-NBD and encapsulating 20  $\mu$ M ATTO 647). The time indicated is relative to the beginning of the recording, which was started as soon as the presence of the LUVs was detected in the green channel close to the selected GUV. Top rows: DPPE-Rh red channel (3D reconstruction of the GUV bottom half); middle rows: DPPE-NBD green channel (3D reconstruction of the bottom half); bottom rows: ATTO 647 grey channel (equatorial cross section). Scale bars: 10  $\mu$ m. Right panels: Graphs of the fluorescence intensity measured on the surface of the GUVs in the green channel (DPPE-NBD) and ratio between the ATTO 647 inside and outside the GUVs in the grey channel. The analyses were performed as described in Fig. 4 in the main text. The brightness (+ 40%) and contrast (- 40%) of the green and red channels were modified to better visualize the beginning of the process. The intensity values of the green channel were corrected for the laser intensity which was different from the one used in the experiments in Figure S7.